nature materials

LETTERS

PUBLISHED ONLINE: 8 FEBRUARY 2009 | DOI: 10.1038/NMAT2382

Towards wafer-size graphene layers by atmospheric pressure graphitization of silicon carbide

Konstantin V. Emtsev[1], Aaron Bostwick[2], Karsten Horn[3], Johannes Jobst[4], Gary L. Kellogg[5], Lothar Ley[1], Jessica L. McChesney[2], Taisuke Ohta[5], Sergey A. Reshanov[4], Jonas Röhrl[1], Eli Rotenberg[2], Andreas K. Schmid[6], Daniel Waldmann[4], Heiko B. Weber[4] and Thomas Seyller[1]*

Graphene, a single monolayer of graphite, has recently attracted considerable interest owing to its novel magneto-transport properties[1–3], high carrier mobility and ballistic transport up to room temperature[4]. It has the potential for technological applications as a successor of silicon in the post Moore's law era[5–7], as a single-molecule gas sensor[8], in spintronics[9–11], in quantum computing[12] or as a terahertz oscillator[13]. For such applications, uniform ordered growth of graphene on an insulating substrate is necessary. The growth of graphene on insulating silicon carbide (SiC) surfaces by high-temperature annealing in vacuum was previously proposed to open a route for large-scale production of graphene-based devices[5,6]. However, vacuum decomposition of SiC yields graphene layers with small grains (30–200 nm; refs 14–16). Here, we show that the *ex situ* graphitization of Si-terminated SiC(0001) in an argon atmosphere of about 1 bar produces monolayer graphene films with much larger domain sizes than previously attainable. Raman spectroscopy and Hall measurements confirm the improved quality of the films thus obtained. High electronic mobilities were found, which reach $\mu = 2{,}000\ \mathrm{cm^2\,V^{-1}\,s^{-1}}$ at $T = 27$ K. The new growth process introduced here establishes a method for the synthesis of graphene films on a technologically viable basis.

The successful development of graphene-based electronic devices depends on a large-scale availability of the material. Several methods for graphene production have been proposed. Mechanical exfoliation[17] leads to isolated, high-quality crystals with dimensions only in the 10 μm range, which questions the practicality of this method. Large, high-quality graphene islands were grown on the surface of transition metals such as Ru(0001) (ref. 18), but this technique requires transfer to an insulating substrate, with methods that have yet to be developed. Liquid-phase exfoliation[19] yields high quantities of monolayer and few-layer graphene. Although this method—in contrast to graphene oxide reduction[20]—prevents the formation of defects, the electrical properties are similar to graphene oxide reduction, indicating poor transport at contacts between the individual graphene sheets.

The preparation of single-layer graphene by the thermal decomposition of silicon carbide (SiC) has been proposed as a viable route for the synthesis of uniform, wafer-size graphene layers for technological applications[5–7]. A considerable advantage of this method is that insulating SiC substrates can be used so that transfer to another insulator is not required. However, the large-scale structural quality is limited at present by the lack of continuity and uniformity of the grown film[15,16]. On the Si-terminated (0001) basal plane, vacuum annealing leads to small graphene domains typically 30–100 nm in diameter, whereas on the C-terminated $(000\bar{1})$ face, larger domains (~200 nm) of multilayered, rotationally disordered graphene have been produced[14]. The small-grain structure is due to morphological changes of the surface in the course of high-temperature annealing. Moreover, decomposition of SiC is not a self-limiting process and, as a result, regions of different film thicknesses coexist, as shown by low-energy electron microscopy[15,16] (LEEM). Such inhomogeneous films do not meet the demands of large-scale device production, which requires larger domains and tighter thickness control. Homogeneous film thickness is particularly important because the electronic structure of the film depends strongly on the number of layers. For example, although monolayer graphene is a gapless semiconductor, a forbidden gap can be induced in bilayer graphene and tuned by an external electrostatic potential[21,22].

Here we demonstrate a method of preparing graphene on SiC(0001) that results in a significantly improved film quality. In Fig. 1, we compare samples prepared by vacuum annealing with samples produced by *ex situ* annealing under an argon atmosphere. Figure 1a–c shows the morphology of the 6H–SiC(0001) surface before and after the formation of a graphene monolayer by annealing in ultrahigh vacuum (UHV) as determined by atomic force microscopy (AFM) and LEEM. The initial 6H–SiC(0001) surface in Fig. 1a, obtained after hydrogen etching, is characterized by wide, highly uniform, atomically flat terraces. The step direction and terrace width (of the order of 300–700 nm) are determined by the incidental misorientation of the substrate surface with respect to the crystallographic (0001) plane. The step height is 1.5 nm, which corresponds to the dimension of the 6H–SiC unit cell in the direction perpendicular to the surface (*c* axis). On defect-free areas of the sample, the terraces typically extend undisturbed over 50 μm in length. The morphology of the surface covered with a monolayer of graphene prepared by vacuum annealing is shown in Fig. 1b. The surface obviously undergoes significant modifications; it is now covered with small pits up to 10 nm in depth, and the original

[1]Lehrstuhl für Technische Physik, Friedrich-Alexander-Universität Erlangen-Nürnberg, Erwin-Rommel-Str. 1, 91058 Erlangen, Germany, [2]Advanced Light Source, Lawrence Berkeley National Laboratory, One Cyclotron Road, Berkeley, California 94720, USA, [3]Department of Molecular Physics, Fritz-Haber-Institut der Max-Planck-Gesellschaft, Faradayweg 4-6, 14195 Berlin, Germany, [4]Lehrstuhl für Angewandte Physik, Friedrich-Alexander-Universität Erlangen-Nürnberg, Staudtstr. 7, 91058 Erlangen, Germany, [5]Sandia National Laboratories, Surface & Interface Sciences Department, PO Box 5800, Albuquerque, New Mexico 87185, USA, [6]National Center for Electron Microscopy, Lawrence Berkeley National Laboratory, One Cyclotron Road, Berkeley, California 94720, USA. *e-mail: thomas.seyller@physik.uni-erlangen.de.

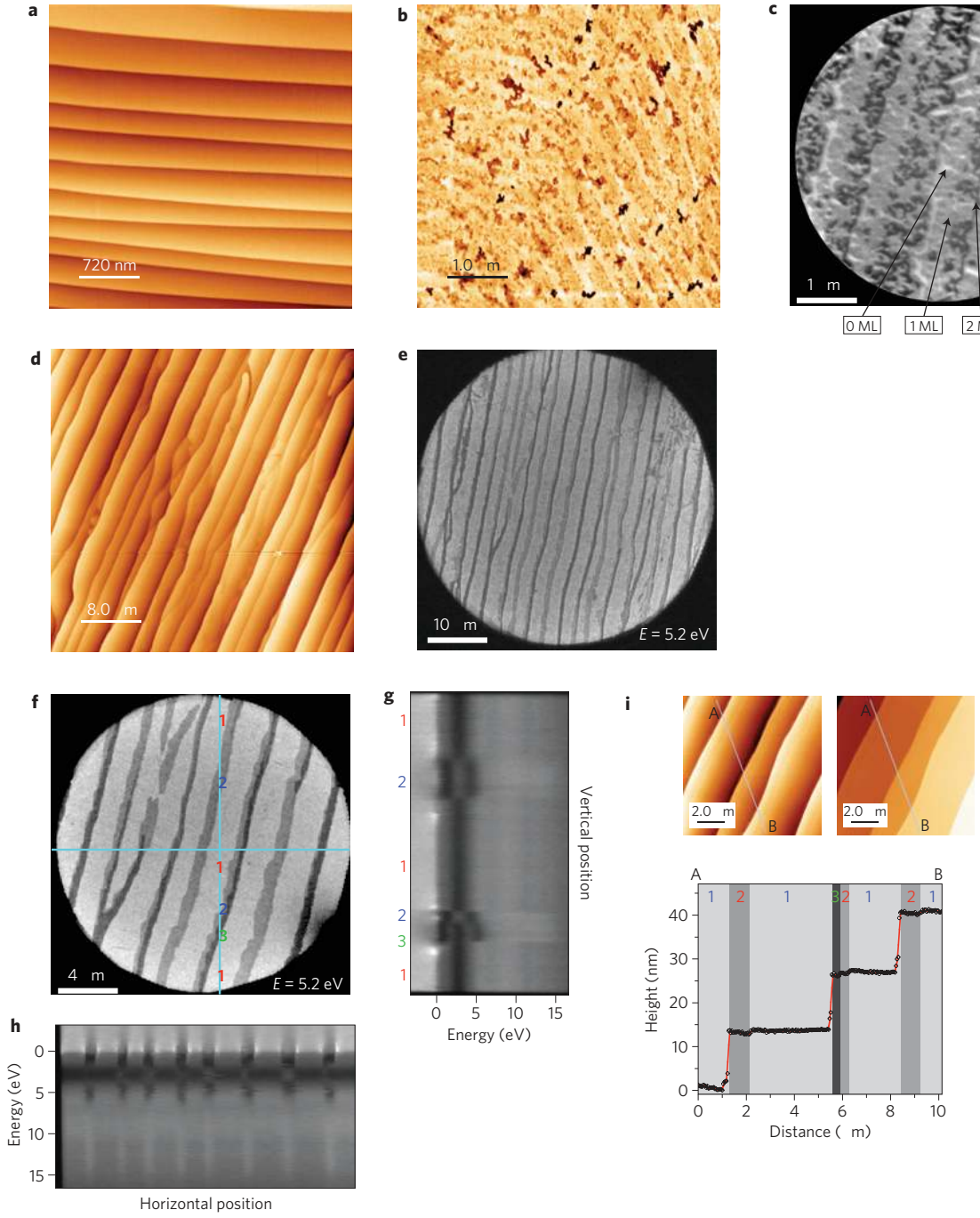

Figure 1 | Morphological changes of 6H–SiC(0001) during graphene growth. a, Initial surface after H-etching imaged by AFM. The step height is 15 Å. **b**, AFM image of graphene on 6H–SiC(0001) with a nominal thickness of 1 ML formed by annealing in UHV at a temperature of about 1,280 °C. **c**, LEEM image of a UHV-grown graphene film on SiC(0001) with a nominal thickness of 1.2 monolayers. The image contrast is due to the locally different layer thickness. Light, medium and dark grey correspond to a local thickness of 0, 1 and 2 ML, respectively. **d**, AFM image of graphene on 6H–SiC(0001) with a nominal thickness of 1.2 ML formed by annealing in Ar ($p = 900$ mbar, $T = 1{,}650$ °C). **e**, LEEM image of a sample equivalent to that of **d** revealing macro-terraces covered with graphene up to 50 μm long and at least 1 μm wide. **f**, Close-up LEEM image revealing monolayer coverage on the terraces and bilayer/trilayer growth at the step edges. **g**,**h**, Electron reflectivity spectra (grey-scale images) taken at the positions indicated by the blue lines in **f**. Monolayer, bilayer and trilayer graphene are readily identified by the presence of 1, 2 or 3 reflectivity minima, respectively. **i**, Close-up AFM images of the film shown in **d**. In the right-hand-side image, the *z* scale was adjusted such that the terraces appear at the same height. The profile shows that small depressions 4 and 8 Å in height exist at the step edges due to second and third layer nucleation.

steps are hardly discernible any longer. This indicates that graphene growth is accompanied by substantial changes in the morphology of the substrate itself, leading to a considerable roughening. As a consequence of this roughening, the graphene layer acquires an inhomogeneous thickness distribution as can be seen in the LEEM image shown in Fig. 1c. The irregularly shaped graphene islands are at most a few hundred nanometres in size, in agreement with X-ray diffraction[14]. Moreover, monolayer graphene areas coexist with graphene bilayer islands as well as with uncovered regions of the $(6\sqrt{3} \times 6\sqrt{3})$ buffer layer[23].

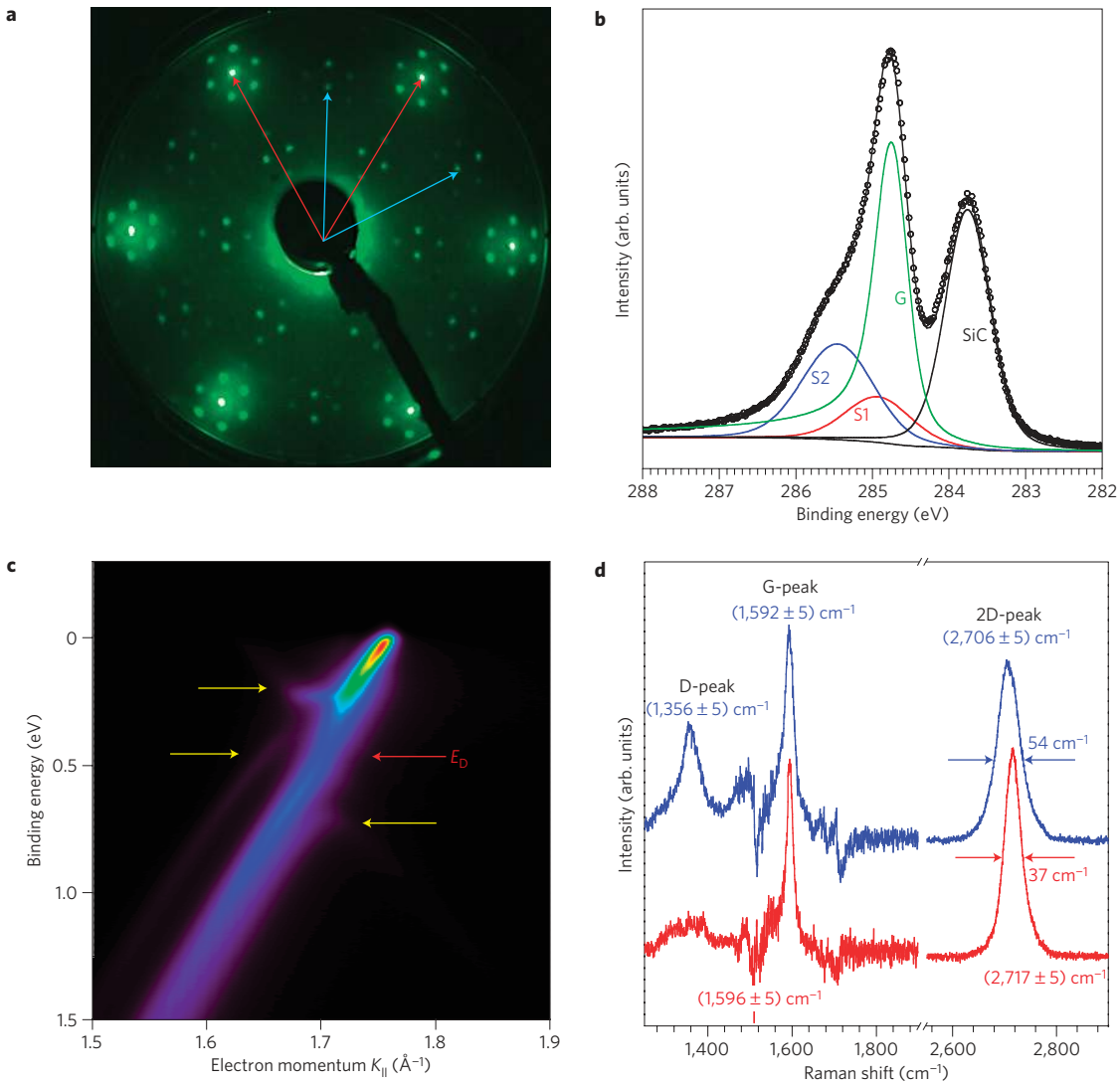

Figure 2 | Atomic and electronic structure of *ex-situ*-grown monolayer graphene. a, LEED pattern at 74 eV showing the diffraction spots due to the SiC(0001) substrate (blue arrows) and the graphene lattice (red arrows). The extra spots are due to the $(6\sqrt{3}\times 6\sqrt{3})$ interface layer. **b**, C1s core-level spectrum measured at a photon energy of 700 eV. The spectrum contains contributions from the SiC substrate (marked SiC), the $(6\sqrt{3}\times 6\sqrt{3})$ interface layer (marked S1 and S2) and from the graphene layer (G) residing on top of the interface layer. **c**, π-bands probed by ARPES in the vicinity of the K-point of the hexagonal Brillouin zone measured along the Γ K-direction. The position of the Dirac energy (E_D) at 0.45 eV below the Fermi energy is consistent with previous reports on UHV-grown graphene on SiC(0001). Faint features marked by yellow arrows signal the presence of small regions of bilayer graphene in agreement with the LEEM results. **d**, Comparison of Raman spectra of Ar-grown (red) and UHV-grown (blue) epitaxial graphene on 6H-SiC(0001). The spectra of the D- and G-line shown here are corrected for the emission of the substrate by subtraction of a reference spectrum[26] (see Supplementary Information).

In stark contrast to the low quality resulting from vacuum graphitization (Fig. 1b), films grown under 900 mbar of argon have a greatly improved surface morphology, as demonstrated by the AFM image in Fig. 1d. Large continuous terraces are found, extending over large distances parallel to the step edges. Step bunching is manifested by the formation of macro-terraces that are a factor of 5–8 times wider than the original terraces. The macro-steps are parallel to the original steps, increase in step height by the same factor and reach average heights of 8–15 nm. Parallel to the steps, uninterrupted macro-terraces more than 50 μm long have been observed.

The thickness distribution of the graphene film grown under an argon atmosphere is determined by LEEM as shown in Fig. 1e,f. A series of spatially resolved LEEM I–V spectra taken along a vertical and a horizontal line in Fig. 1f is shown in Fig. 1g,h. The layer thickness is easily determined from the number of minima in the individual spectra; the LEEM image taken at a particular energy shows stripes that follow in width and orientation the macro-terraces with a contrast that is determined by the graphene layer thickness[15,16]. Hence, we can unambiguously conclude that except for narrow stripes at the edges, the large atomically flat macro-terraces are homogeneously covered with a graphene monolayer. The domain size of monolayer graphene is significantly larger than that of the vacuum-annealed samples as a comparison between Fig. 1c,f shows. In fact, the domain size seems to be limited only by the length and width of the SiC terraces. Narrower, darker regions at the downward edges of the terraces correspond to bilayer and in some cases trilayer graphene (see region 3 in Fig. 1f). In the AFM image, these regions (see Fig. 1i) appear as small depressions of around 0.5 nm and 1 nm amplitude located at the very edge of the macro-step. This indicates that the nucleation of new graphene layers starts at step edges of the substrate surface.

The structural and electronic properties of Ar-grown graphene layers were probed by low-energy electron diffraction (LEED), photoelectron spectroscopy and Raman spectroscopy as shown in Fig. 2. Although these methods alone cannot assess the morphological quality of the sample surface on a large scale, they provide extra information as detailed below. The LEED pattern (Fig. 2a) demonstrates that the graphene layer is well ordered and aligned with respect to the substrate, such that the basal plane unit vectors of graphene and SiC subtend an angle of 30°. The C1*s* core-level spectrum (Fig. 2b) shows the characteristic signals of the SiC substrate, the non-metallic ($6\sqrt{3} \times 6\sqrt{3}$) interface layer (buffer layer) that decouples the electronic structure of graphene from the substrate and the graphene monolayer that lies on top of the buffer layer, in agreement with vacuum-grown films[23]. Angle-resolved photoelectron spectra (Fig. 2c) reveal the characteristic band structure of monolayer graphene[24]. Note that, as for vacuum-grown layers[24], the Dirac point (E_D) is shifted below the Fermi level (E_F) owing to electron doping ($n \approx 1.1 \times 10^{13}$ cm^{-2}) from the substrate. Figure 2d compares Raman spectra of epitaxial graphene grown in UHV and in Ar. For the Ar-grown sample, the G- and 2D-lines are observed at 1,596 and 2,717 cm^{-1}, respectively. The 2D-line consists of a narrow peak (full-width at half-maximum: 37 cm^{-1}), which is characteristic of monolayer graphene[25,26]. Its blueshift (38 cm^{-1}) with respect to exfoliated graphene[25] was previously explained by compressive strain[26]. The UHV-grown sample shows a broader and less symmetric 2D-peak, which clearly indicates that it contains more than one component in agreement with the broader thicknesses distribution determined by LEEM. Its smaller blueshift (29 cm^{-1}) is probably due to a partial strain relief of the smaller domains. A strong D-peak at 1,356 cm^{-1} signals the presence of many defects and domain boundaries. Therefore, although our epitaxial growth process results in a marked improvement in surface morphology, all other properties such as orientation with respect to the substrate, electronic structure and charge carrier density remain unaltered as compared to vacuum-grown layers.

What is the reason for the observed improvement of the surface morphology of the Ar-annealed samples compared with the samples annealed in UHV? From the data in Fig. 1, it is clear that the surface undergoes considerable morphological changes at the temperature where graphitization occurs. The large roughness of the UHV-annealed samples suggests that the surface is far from equilibrium, such that a transformation to a smooth morphology cannot be achieved under these conditions. The key factor in achieving an improved growth is the significantly higher annealing temperature of 1,650 °C that is attainable for graphene formation under argon at a pressure of 900 mbar as compared with 1,280 °C in UHV. Graphene formation is the result of Si evaporation from the substrate. For a given temperature, the presence of a high pressure of argon leads to a reduced Si evaporation rate because the silicon atoms desorbing from the surface have a finite probability of being reflected back to the surface by collision with Ar atoms, as originally pointed out by Langmuir[27,28]. Indeed, in the presence of the Ar atmosphere, no sublimation of Si from the surface is observed at temperatures up to 1,500 °C, whereas Si desorption commences at 1,150 °C in vacuum (see Supplementary Information). The significantly higher growth temperature thus attained results in an enhancement of surface diffusion such that the restructuring of the surface is completed before graphene is formed. Ultimately, this leads to the markedly improved surface morphology that we observe here. The macro-step structure is also responsible for the tighter thickness control. New graphene layers start to grow from the step edges; hence having fewer steps along well-defined crystallographic directions reduces the nucleation density of multilayer graphene.

To evaluate the electronic quality of our graphene layers, we determined the carrier mobility of monolayer epitaxial graphene on SiC(0001) using Hall effect measurements. Table 1 compares carrier mobilities for Ar-grown and UHV-grown samples measured on Hall bars and in van der Pauw geometry. The mobilities obtained by Ar annealing are higher by about a factor of two at 300 K and by three at 27 K. This suggests that the large number of domain boundaries in vacuum-grown graphene has a major negative impact on carrier mobility. On the other hand, no significant difference in electron mobility was observed between the two geometries, indicating that the step edges have a minor role, similar to graphene field-effect transistors in multilayer graphene[29]. Note that scanning tunnelling microscopy has provided evidence that graphene layers are continuous over step edges[5,30] and graphene field-effect transistors with multilayer graphene[29] show no dependence on the alignment with respect to substrate steps. However, extra experiments with Hall bars aligned parallel and perpendicular to steps will be carried out to unambiguously clarify the effect of steps on carrier mobility. The electron density determined by the Hall measurements is $n \approx 1 \times 10^{13}$ cm^{-2}, in agreement with the angle-resolved photoelectron spectroscopy (ARPES) measurements. Hence, we compare the measured mobilities with exfoliated monolayer graphene on SiO_2 in the high doping limit, where values of the order of 10,000 cm^2 V^{-1} s^{-1} are reported for $n \approx 5 \times 10^{12}$ cm^{-2} (refs 1,2). For epitaxial graphene on SiC(0001), other groups reported values of 1,200 cm^2 V^{-1} s^{-1} for multilayered graphene[5,29].

Table 1 | Hall mobilities (in cm^2 V^{-1} s^{-1}) for Hall bars and van der Pauw structures on UHV- and Ar-grown graphene measured at $T = 300$ and 27 K.

Method	Structure	300 K	27 K
Ar	Hall bar	900	1,850
	Van der Pauw	930	2,000
UHV	Hall bar	470	—
	Van der Pauw	550	710

In summary, we have shown that the growth of epitaxial graphene on SiC(0001) in an Ar atmosphere close to atmospheric pressure provides morphologically superior graphene layers in comparison with vacuum graphitization. Extensive step bunching taking place during processing yields arrays of parallel terraces up to 3 μm wide and more than 50 μm long. The terraces are essentially completely and homogeneously covered with a monolayer of graphene. At present, downward step edges, where the initiation of second- and third-layer graphene growth is detected, are prohibiting an even larger extension of the monolayer graphene domains. Because the substrate step direction and step width are determined by the magnitude and azimuthal orientation of the surface misorientation with respect to major crystallographic directions, a proper choice of these parameters controls terrace width and length and hence the ultimate size of the graphene domains. An improved substrate quality in terms of crystallographic orientation is therefore expected to lead to further improvements. In comparison to UHV treatment, the technique presented here is much closer to standard preparation conditions in semiconductor manufacturing, permitting the use of standard chemical vapour deposition equipment for the fabrication of graphene layers. All necessary processing steps (hydrogen etching and graphene synthesis) can be carried out in a single reactor. Electrical measurements confirm the improved film quality.

Methods

Graphene layers were synthesized on commercial, nominally on-axis oriented wafers of 6H–SiC(0001) purchased from SiCrystal AG. For experiments concerning the morphology of the surface and for the surface science experiments, we used

nitrogen-doped substrates with a doping concentration of $1–2 \times 10^{18}$ cm^{-3}. For electrical measurements (see below), semi-insulating 6H–SiC(0001) was used. Before graphene epitaxy, the samples were etched in hydrogen (grade 5.0, $p = 1$ bar, $T = 1{,}550$ °C, $t = 15$ min) to remove surface polishing damage. Graphene growth was carried out in a vertical cold-wall reactor comprising a double-walled, water-cooled quartz tube and a graphite susceptor in a slow flow of argon (purity 5.0). Heating and cooling rates were 2–3 °C per second. Typical annealing time was 15 min. A wide range of annealing temperatures from 1,500 to 2,000 °C and reactor gas pressures from 10 to 900 mbar were tested. However, except for very low pressures studied, the morphology of the surface after graphene formation in an Ar atmosphere is generally much smoother and the graphene domain size much larger compared with vacuum annealing.

Surface composition and graphene thicknesses were determined from core-level photoelectron spectroscopy by means of a Specs PHOIBOS150 analyser in combination with a monochromatized Al Kα source with an energy resolution of ~350 meV. Owing to the chemical inertness of graphene, the samples can be easily transported through air. As-prepared graphene samples showed no detectable oxygen on the surface (below 1% of a monolayer) even after air exposure for about 1 h. Prolonged air exposure, however, leads to a fractional layer of physisorbed hydrocarbons and water, which can be removed by annealing in vacuum at around 600 °C. ARPES measurements were carried out at the Advanced Light Source using a Scienta R4000 analyser with an overall resolution of ~25 meV at a photon energy of 94 eV and at a sample temperature of 20 K. Core-level measurements were carried out at BESSY-II with a Specs PHOIBOS150 analyser with a resolution of ~125 meV at a photon energy of 700 eV and at room temperature. The surface morphology was probed by AFM in non-contact mode. LEEM measurements at room temperature with a spatial resolution better than 10 nm were carried out at Sandia National Laboratory and at the National Center for Electron Microscopy, Lawrence Berkeley National Laboratory. The laterally averaged graphene thickness determined by LEEM is in perfect agreement with the average layer thickness obtained by X-ray photoelectron spectroscopy. The crystal structure of the films was monitored by LEED.

Raman spectra were measured at room temperature by means of a triple spectrometer equipped with a liquid-nitrogen-cooled CCD (charge-coupled device) detector. A frequency-doubled $NdYVO_4$ laser with a wavelength of 532 nm was used for excitation. A confocal optical microscope was used to record micro-Raman spectra with a spatial resolution of 2 μm.

For the electrical characterization, the samples were patterned by two electron beam lithography steps. The first step defined the graphene film (undesired areas were etched with oxygen plasma). A second step defined the contact pads, which consist of a thermally evaporated Ti/Au double layer, patterned by a standard lift-off technique. Two different geometries were investigated: square graphene films (100 μm × 100 μm) with contact pads at the four corners for van der Pauw measurements as well as Hall bars (4 μm × 50 μm) placed along macro-terraces. The measurements were carried out in a continuous-flow cryostat (sample in vacuum), using magnetic fields of ±0.66 T at temperatures between 300 and 27 K.

Received 14 July 2008; accepted 7 January 2009; published online 8 February 2009

References

1. Novoselov, K. S. *et al.* Two-dimensional gas of massless Dirac fermions in graphene. *Nature* **438**, 197–200 (2005).
2. Zhang, Y. B., Tan, Y. W., Stormer, H. L. & Kim, P. Experimental observation of the quantum Hall effect and Berry's phase in graphene. *Nature* **438**, 201–2004 (2005).
3. Novoselov, K. S. *et al.* Unconventional quantum Hall effect and Berry's phase of 2π in bilayer graphene. *Nature Phys.* **2**, 177–180 (2006).
4. Novoselov, K. S. *et al.* Room-temperature quantum Hall effect in graphene. *Science* **315**, 1379 (2007).
5. Berger, C. *et al.* Ultrathin epitaxial graphite: 2D electron gas properties and a route toward graphene-based nanoelectronics. *J. Phys. Chem. B* **108**, 19912–19916 (2004).
6. Berger, C. *et al.* Electronic confinement and coherence in patterned epitaxial graphene. *Science* **312**, 1191–1196 (2006).
7. Geim, A. K. & Novoselov, K. S. The rise of graphene. *Nature Mater.* **6**, 183–191 (2007).
8. Schedin, F. *et al.* Detection of individual gas molecules adsorbed on graphene. *Nature Mater.* **6**, 652–655 (2007).
9. Son, Y.-W., Cohen, M. L. & Louie, S. G. Half-metallic graphene nanoribbons. *Nature* **444**, 347–349 (2006).
10. Trauzettel, B., Bulaev, D. V., Loss, D. & Burkard, G. Spin qubits in graphene quantum dots. *Nature Phys.* **3**, 192–196 (2007).
11. Yokoyama, T. Controllable spin transport in ferromagnetic graphene junctions. *Phys. Rev. B* **77**, 073413 (2008).
12. Fal'ko, V. I. Graphene: Quantum information on chicken wire. *Nature Phys.* **3**, 151–152 (2007).
13. Rana, F. Graphene terahertz plasmon oscillators. *IEEE Trans. Nanotech.* **7**, 91–99 (2008).
14. Hass, J. *et al.* Highly ordered graphene for two dimensional electronics. *Appl. Phys. Lett.* **89**, 143106 (2006).
15. Hibino, H. *et al.* Microscopic thickness determination of thin graphite films formed on SiC from quantized oscillation in reflectivity of low-energy electrons. *Phys. Rev. B* **77**, 075413 (2008).
16. Ohta, T. *et al.* Morphology of graphene thin film growth on SiC(0001). *New J. Phys.* **10**, 023034 (2008).
17. Novoselov, K. S. *et al.* Two-dimensional atomic crystals. *Proc. Natl Acad. Sci. USA* **102**, 10451–10453 (2005).
18. Sutter, P. W., Flege, J.-I. & Sutter, E. A. Epitaxial graphene on ruthenium. *Nature Mater.* **7**, 406–411 (2008).
19. Hernandez, Y. *et al.* High-yield production of graphene by liquid-phase exfoliation of graphite. *Nature Nanotech.* **3**, 563–568 (2008).
20. Gomez-Navarro, C. *et al.* Electronic transport properties of individual chemically reduced graphene oxide sheets. *Nano Lett.* **7**, 3499–3503 (2007).
21. McCann, E. & Fal'ko, V. I. Landau-level degeneracy and quantum Hall effect in a graphite bilayer. *Phys. Rev. Lett.* **96**, 086805 (2006).
22. Ohta, T. *et al.* Controlling the electronic structure of bilayer graphene. *Science* **313**, 951–954 (2006).
23. Emtsev, K. V. *et al.* Interaction, growth, and ordering of epitaxial graphene on SiC{0001} surfaces: A comparative photoelectron spectroscopy study. *Phys. Rev. B* **77**, 155303 (2008).
24. Bostwick, A. *et al.* Quasiparticle dynamics in graphene. *Nature Phys.* **3**, 36–40 (2007).
25. Ferrari, A. C. *et al.* Raman spectrum of graphene and graphene layers. *Phys. Rev. Lett.* **97**, 187401 (2006).
26. Röhrl, J. *et al.* Raman spectra of epitaxial graphene on SiC(0001). *Appl. Phys. Lett.* **92**, 201918 (2008).
27. Langmuir, I. Convection and conduction of heat in gases. *Phys. Rev. (Series I)* **34**, 401–422 (1912).
28. Fonda, G. R. Evaporation of tungsten under various pressures of argon. *Phys. Rev. (Series II)* **31**, 260–266 (1928).
29. Kedzierski, J. *et al.* Epitaxial graphene transistors on SiC substrates. *IEEE Trans. Electron Devices* **55**, 2078–2085 (2008).
30. Seyller, Th. *et al.* Structural and electronic properties of graphite layers grown on SiC(0001). *Surf. Sci.* **600**, 3906–3911 (2006).

Acknowledgements

We thank F. El Gabaly for assistance with the LEEM measurements and M. Gick for help with the sample preparation. We gratefully acknowledge support by the DFG under contract SE 1087/5-1, contract WE 4542-5-1, and within the Cluster of Excellence 'Engineering of Advanced Materials' (www.eam.uni-erlangen.de) at the Friedrich-Alexander-Universität Erlangen-Nürnberg, by BaCaTeC, and by the BMBF under contract 05 ES3XBA/5. A part of the work was carried out at Sandia National Laboratories, a multiprogram laboratory operated by Sandia Corporation, a Lockheed Martin company, for the United States Department of Energy, Office of Basic Energy Sciences, Division of Materials Science and Engineering, under Contract No. DE-AC04-94AL85000. The work carried out at the Advanced Light Source was supported by the Director, Office of Science, Office of Basic Energy Sciences, of the US Department of Energy under Contract No. DE-AC03-76SF00098.

Author contributions

K.V.E. developed the growth process of large-area graphene with the help of S.A.R. AFM measurements were done by K.V.E. and T.O. T.O. and A.S. carried out the LEEM measurements with the help of G.K. Photoelectron spectroscopy measurements were carried out by K.V.E., T.S., A.B., J.L.M., E.R. and K.H. J.J., D.W. and H.B.W carried out lithography and electrical measurements. J.R. carried out Raman measurements. T.S., K.V.E. and L.L. wrote the manuscript with revision and input from all other co-authors.

Additional information

Supplementary Information accompanies this paper on www.nature.com/naturematerials. Reprints and permissions information is available online at http://npg.nature.com/reprintsandpermissions. Correspondence and requests for materials should be addressed to T.S.